

Implications for (d, p) reaction theory from nonlocal dispersive optical model analysis of $^{40}\text{Ca}(d, p)^{41}\text{Ca}$

S. J. Waldecker¹ and N. K. Timofeyuk²¹*Department of Chemistry and Physics, University of Tennessee at Chattanooga, 615 McCallie Avenue, Chattanooga, Tennessee 37403, USA*²*Department of Physics, Faculty of Engineering and Physical Sciences, University of Surrey, Guildford, Surrey GU2 7XH, United Kingdom*

(Received 31 May 2016; published 9 September 2016)

The nonlocal dispersive optical model (NLDOM) nucleon potentials are used for the first time in the adiabatic analysis of a (d, p) reaction to generate distorted waves both in the entrance and exit channels. These potentials were designed and fitted by Mahzoon *et al.* [*Phys. Rev. Lett.* **112**, 162503 (2014)] to constrain relevant single-particle physics in a consistent way by imposing the fundamental properties, such as nonlocality, energy-dependence and dispersive relations, that follow from the complex nature of nuclei. However, the NLDOM prediction for the $^{40}\text{Ca}(d, p)^{41}\text{Ca}$ cross sections at low energy, typical for some modern radioactive beam ISOL (isotope separation online) facilities, is about 70% higher than the experimental data despite being reduced by the NLDOM spectroscopic factor of 0.73. This overestimation comes most likely either from insufficient absorption or due to constructive interference between ingoing and outgoing waves. This indicates strongly that additional physics arising from many-body effects is missing in the widely used current versions of (d, p) reaction theories.

DOI: [10.1103/PhysRevC.94.034609](https://doi.org/10.1103/PhysRevC.94.034609)

I. INTRODUCTION

One-nucleon transfer reactions have been a tool for nuclear spectroscopic studies for half of a century. Today, they are used in experiments with radioactive beams, and among them the (d, p) reactions are perhaps the most popular choice. Analysis of these reactions relies on (d, p) reaction theory, which is traditionally either the distorted-wave Born approximation (DWBA) [1] or adiabatic distorted wave approximation (ADWA) [2], the latter being a computationally inexpensive way of taking into account deuteron breakup. The deuteron breakup means that the (d, p) amplitude should contain the $A + n + p$ degrees of freedom explicitly, which requires solving the $A + n + p$ three-body Schrödinger equation. Several methods exist to solve this equation exactly, the CDCC [3,4] and the Faddeev approach [5] being the most used. The usual assumption in these calculations is that the $A + n + p$ Hamiltonian contains the p - A and n - A potentials (often taken at half the deuteron incident energy) that describe nucleon elastic scattering. However, it has been shown in [6] that the n - A and p - A potentials for the $A + n + p$ problem are very complicated objects which depend on the position and the energy of the third nucleon and are not equal to optical potentials taken at half the deuteron energy. It was also shown in [6] that in the case of (d, p) reactions the averaging over the first Weinberg component (which is the same as making the adiabatic approximation) results in a simple prescription for choosing the n - A and p - A potentials appropriate for analysis of (d, p) reactions. This prescription is possible due to the main contribution to the (d, p) amplitude coming from small n - p separations.

The prescription in [6] says that, within the Feshbach formalism, the n - A and p - A potentials should be nonlocal energy-dependent potentials evaluated at half the deuteron incident energy plus half of the n - p kinetic energy in the deuteron averaged over the n - p potential, which is about 57 MeV. After evaluation of these potentials, they should be

treated as energy independent and nonlocal. A simple recipe to include such potentials in the available (d, p) reaction scheme, based on the local energy approximation, is given in [7].

At the time when [6] was written, only one energy-dependent nonlocal potential had been known [8], derived from Watson multiple scattering theory. It has an energy-independent real part and an energy-dependent imaginary potential. Soon after the publication of [6], a nonlocal version of the dispersive optical model (NLDOM) became available for ^{40}Ca [9]. The nonlocal structure of NLDOM is more complicated than that from previous nonlocal optical potentials in that it is described by seven different nonlocality parameters. Based on the nucleon self-energy from Green's function many-body theory, the NLDOM potential contains both real and imaginary dynamic terms that are connected through a dispersion relation, which enforces causality and links the negative and positive energy regions. This dispersion relation is important for constraining the NLDOM parameters with both scattering and bound-state data while simultaneously providing a good description of these data. The potential from Ref. [8] was also constrained with both scattering and bound-state data but without incorporating the dispersion relation.

In this paper, we analyze the $^{40}\text{Ca}(d, p)^{41}\text{Ca}$ reaction at 11.8 MeV using NLDOM to generate the distorting potentials in both the entrance and exit channels. The NLDOM potential has already been used in [10] to calculate the $^{40}\text{Ca}(p, d)^{39}\text{Ca}$ cross sections but only within the DWBA (which means neglecting deuteron breakup) and no comparison to the experimental data was made. Our choice of the reaction is due to the availability of the p - ^{40}Ca and n - ^{40}Ca optical potentials needed to construct the d - ^{40}Ca potential. The choice of the deuteron energy is due to several radioactive beams facilities existing in the world that use this low-energy range. Also, it is this low-energy range where the dispersive relations cause the most prominent effects in the energy behavior of the optical potential. In addition, at these energies, spin-orbit effects and

finite range effects can be neglected and the prescription from [6] should be valid.

In Sec. II, we review the NLDOM and show that, similar to the standard Perey-Buck case, a local-equivalent potential exists for NLDOM and a generalization of the Perey factor can be introduced. In a similar fashion, we show in Sec. III that the d - ^{40}Ca distorting potential can be constructed by extending the local scheme proposed in [7] to the case with several nonlocality parameters. We summarize the adiabatic approximation in lowest order and introduce first-order corrections. In Sec. IV we calculate the cross section of the $^{40}\text{Ca}(d,p)^{41}\text{Ca}$ reaction at 11.8 MeV and show that, using the prescription from [6], the NLDOM strongly overestimates the experimental data. In Sec. V, we discuss the implications for the (d,p) reaction theory following from our analysis.

II. NONLOCAL DOM POTENTIAL AND NUCLEON SCATTERING

The NLDOM potential from Ref. [9] models the irreducible nucleon self-energy $\Sigma(\mathbf{r}, \mathbf{r}'; E)$ with real and imaginary parts that are both explicitly nonlocal. The potential contains eight terms, which were constrained with both bound-state and scattering data associated with ^{40}Ca . It is written in the form

$$\begin{aligned} \Sigma(\mathbf{r}, \mathbf{r}'; E) = & U_{HF}^{\text{vol}1}(\tilde{r})H(\mathbf{x}; \beta_{\text{vol}1}) + U_{HF}^{\text{vol}2}(\tilde{r})H(\mathbf{x}; \beta_{\text{vol}2}) \\ & + U_{HF}^{\text{wb}}(\tilde{r})H(\mathbf{x}; \beta_{\text{wb}}) + U_{dy}^{\text{sur}+}(\tilde{r}; E)H(\mathbf{x}; \beta_{\text{sur}+}) \\ & + U_{dy}^{\text{sur}-}(\tilde{r}; E)H(\mathbf{x}; \beta_{\text{sur}-}) \\ & + U_{dy}^{\text{vol}+}(\tilde{r}; E)H(\mathbf{x}; \beta_{\text{vol}+}) \\ & + U_{dy}^{\text{vol}-}(\tilde{r}; E)H(\mathbf{x}; \beta_{\text{vol}-}) + U_{so}(r; E), \end{aligned} \quad (1)$$

where $\tilde{r} = |\mathbf{r} + \mathbf{r}'|/2$ and $\mathbf{x} = \mathbf{r}' - \mathbf{r}$. Following Perey and Buck [11], the nonlocality function H is assumed to be of the form

$$H(\mathbf{x}; \beta) = \exp(-\mathbf{x}^2/\beta^2)/(\pi^{3/2}\beta^3), \quad (2)$$

where β is the nonlocality range.

In Eq. (1) the U_{HF} terms represent the static part of the self-energy and are purely real. For this reason, these terms are referred to as parts of the Hartree-Fock (HF) potential, but technically they do not form the true HF potential, because in practice a subtracted dispersion relationship is used [9]. The U_{dy} terms represent the dynamic part of the self-energy and are complex. The real part of the dynamic self-energy is determined completely from the dispersion integral of the imaginary part. The dynamic self-energy consists of surface and volume terms, and these have different nonlocalities for energies above the Fermi energy E_F (denoted with a “+” sign) and energies below E_F (denoted by a “-” sign). The inclusion of several nonlocality parameters was based on the microscopic calculation in Ref. [12], which indicated different degrees of nonlocality in different energy regions. Table I shows the value of each nonlocality parameter. Note that some of these parameters are about twice as large as those known from traditional Perey-Buck potentials. The U_{so} term is the spin orbit potential, which was assumed to be local. It has a

TABLE I. NLDOM nonlocality parameters.

Parameter	Nonlocality (fm)
$\beta_{\text{vol}1}$	0.84
$\beta_{\text{vol}2}$	1.55
β_{wb}	1.04
$\beta_{\text{sur}+}$	0.94
$\beta_{\text{sur}-}$	2.07
$\beta_{\text{vol}+}$	0.64
$\beta_{\text{vol}-}$	0.81

weak energy dependence that only becomes important at high energies.

Overlap functions can also be generated with the dispersive optical model. For discrete states in the $A + 1$ and $A - 1$ systems, one can show that these overlap functions obey a Schrödinger-like equation [13] with the nucleon self-energy taking the role of an effective potential. In order to use the NLDOM overlap function in the analysis of $^{40}\text{Ca}(d,p)^{41}\text{Ca}$ reactions, the calculated binding energy of the $0f_{7/2}$ neutron level in ^{40}Ca must match the experimental one of 8.36 MeV. However, in [9], such a constraint was not employed. For the purposes of this study, some of the parameters were refit in order to reproduce the experimental binding energy of the $0f_{7/2}$ neutron level. Only the parameters associated with the U_{HF} terms were refit, and they were constrained by elastic scattering, charge density, and energy level data. All other parameters were unchanged. The new parameters are shown in Table II and compared with those from the analysis in [9]. The quality of the new fit is comparable to that obtained in [9].

The nonlocal terms in Eq. (1) can be written more succinctly as

$$\Sigma_N(\mathbf{r}, \mathbf{r}'; E) = \sum_i U_{N_A,i}(\tilde{r})H_i(x), \quad (3)$$

where the energy dependence of the dynamic terms is implied, and $N = p, n$ for proton and neutron potentials, respectively.

In this paper we will construct an effective local model for the deuteron-target adiabatic potential using NLDOM. Therefore, we first evaluate the effective local potential model for nucleon scattering. Following the procedure in [11] for transforming a nonlocal potential to a local equivalent, one

TABLE II. Adjusted HF parameters used in the present fit. For a description of these parameters, refer to [9].

Parameter	New value	Old value
V_{HF}^0 (MeV)	106.15	100.06
r_{HF} (fm)	1.14	1.10
a_{HF} (fm)	0.58	0.68
$\beta_{\text{vol}1}$ (fm)	0.84	0.66
$\beta_{\text{vol}2}$ (fm)	1.55	1.56
x_1	0.48	0.48
V_{wb}^0 (MeV)	12.5	15.0
ρ_{wb} (fm)	2.06	1.57
β_{wb} (fm)	1.04	1.10

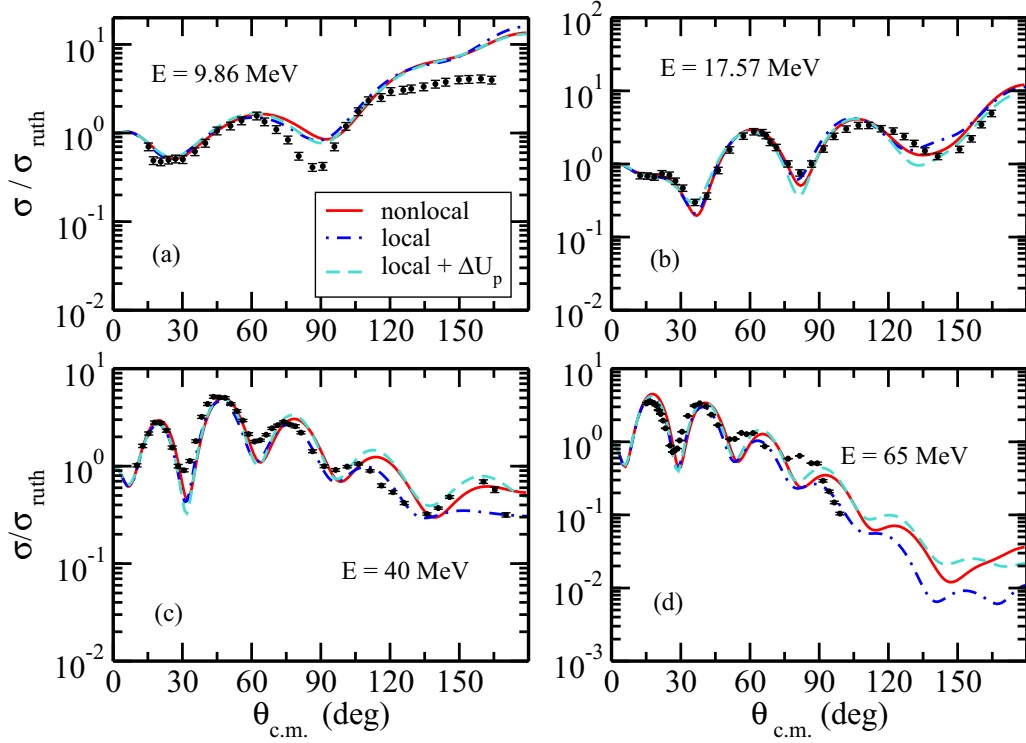


FIG. 1. Differential cross sections normalized by the Rutherford cross section for proton scattering on ^{40}Ca at (a) 9.86 MeV, (b) 17.57 MeV, (c) 40 MeV, and (d) 65 MeV, calculated using the fully nonlocal DOM potential (solid), using the local potential U_{loc} from Eq. (4) with the Coulomb and spin-orbit potentials included (dot-dashed), and using this equivalent local potential but with the correction ΔU_p included as well (dashed). These are compared with the experimental data (dots).

finds that for a nonlocal potential with multiple nonlocalities of the Perey-Buck type the local-equivalent potential can be found by solving the transcendental equation

$$U_{\text{loc}}(r) = \sum_i U_{NA,i}(r) \exp \left[-\frac{\mu_N \beta_i^2}{2\hbar^2} [E - U_{\text{loc}}(r)] \right], \quad (4)$$

where μ_N is the reduced mass of the $N + A$ system. This equation is obtained in the lowest order of the expansion of $\Sigma_N(\mathbf{r}, \mathbf{r}'; E)$ over x and corrections to any order can be built systematically using developments from [14]. In particular, the first-order correction is

$$\Delta U_N = \frac{\hbar^2}{\mu_N} \left[\left(\frac{\nabla f}{f} \right)^2 - \frac{1}{2} \frac{\nabla^2 f}{f} \right], \quad (5)$$

where the function $f(r)$ is the Perey factor explained below. For proton scattering, Eq. (4) must be corrected by reducing the center-of-mass energy E in the right-hand side of Eq. (4) by the local Coulomb interaction $V_{\text{coul}}(r)$.

According to [14], the local spin-orbit term must also be corrected when transforming to a local-equivalent potential. For the present case of a potential with multiple nonlocality parameters, the new spin-orbit term, U_{so}^{le} , of the local-equivalent potential is

$$U_{so}^{le} = U_{so}/(1 - U_1) \quad (6)$$

where

$$U_1 = \left(1 - \sum_i \frac{\mu_N \beta_i^2}{2\hbar^2} U_{NA,i}(r) G_i(r, E) \right) \quad (7)$$

and

$$G_i(r, E) = \exp \left[-\frac{\mu_N \beta_i^2}{2\hbar^2} [E - U_{\text{loc}}(r)] \right]. \quad (8)$$

Figure 1 compares proton scattering differential cross sections (normalized by the Rutherford cross section) determined from solving the NLDOM scattering problem exactly using the iterative procedure outlined in Ref. [15] and from solving the local-equivalent problem. Both the Coulomb and spin-orbit corrections are included. The experimental data are from Refs. [16–19]. Aside from small deviations at large angles, the results from using Eq. (4) are very similar to the exact solutions. The results from including ΔU_p are also shown. Overall, this correction improves the correspondence between the exact and approximate solutions of the nonlocal problem for angles $\theta \approx 40^\circ$ and above.

For Perey-Buck potentials with one nonlocality parameter the N - A wave function obtained from the phase-equivalent local model defined by a potential $U(r) = U_{\text{loc}} + \Delta U_N$ differs in the nuclear interior from the exact N - A wave function by the Perey factor [14]

$$f(r) = \exp \left[\frac{\mu_N \beta^2}{4\hbar^2} U_{\text{loc}}(r) \right]. \quad (9)$$

Elastic scattering observables do not depend on the Perey factor. Transfer cross sections may depend on it if they are not peripheral. In the particular case of $^{40}\text{Ca}(d,p)^{41}\text{Ca}$, the internal part contributes up to 20% [20] for the energy being considered, and this contribution is more important in the DWBA than in the ADWA. One can show it is also possible to derive the Perey factor for optical potentials with multiple nonlocalities such as in NLDOM. In this case the Perey factor is

$$f(r) = \exp \left[\frac{\mu_N \beta_{\text{eff}}^2(r)}{4\hbar^2} U_{\text{loc}} \right], \quad (10)$$

where

$$\beta_{\text{eff}}^2(r) = -U_{\text{loc}}^{-1}(r) \int_r^\infty dr_1 \frac{\sum_i \beta_i^2 U'_{NA,i}(r_1) G_i(r_1, E)}{1 - U_1(r_1, E)}. \quad (11)$$

This Perey factor has some effective r -dependent range β_{eff} , which can be complex. The real and imaginary parts are shown in Fig. 2 for the case of p - ^{40}Ca elastic scattering at several proton energies. The imaginary part is small and has a negligible effect on the (d,p) cross sections. We note that β_{eff} decreases with energy. This decrease reflects the fact that $\beta_{\text{sur}+}$ is larger than $\beta_{\text{vol}+}$. Since the volume imaginary potential dominates at higher energies, the term in Eq. (4) with $\beta_i = \beta_{\text{vol}+}$ becomes more important with increasing energy. This term also seems to dominate at large r , as $\text{Re } \beta_{\text{eff}}$ converges to $\beta_{\text{vol}+} = 0.64$ fm for all energies.

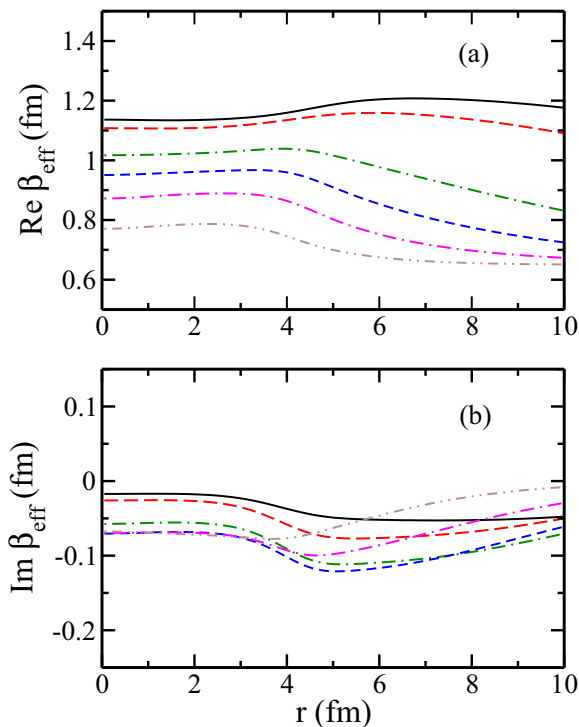


FIG. 2. (a) Real and (b) imaginary parts of β_{eff} for $E = 9.86$ MeV (solid), 17.57 MeV (long dashed), 40 MeV (long dot-dashed), 65 MeV (short dashed), 100 MeV (short dot-dashed), and 200 MeV (dot-dot-dashed).

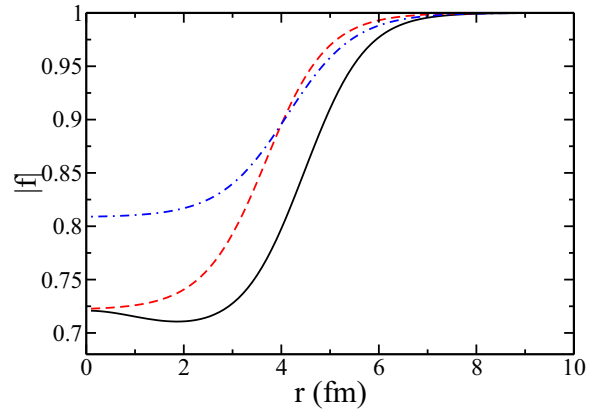


FIG. 3. Absolute value of the Perey factor evaluated at $E_{cm} = 17.37$ MeV for NLDOM (solid), LDOM (dashed), and CH89 (dot-dashed).

The Perey factor for NLDOM is shown in Fig. 3, evaluated at the energy $E_p = 17.37$ MeV, which is the center of mass energy for the outgoing proton in the $^{40}\text{Ca}(d,p)^{41}\text{Ca}$ reaction with $E_d = 11.8$ MeV (in the laboratory frame). It is compared to the Perey factor of an earlier version of the DOM [21] that is purely local (LDOM). This Perey factor will be used in Sec. IV. It is given by [22,23]

$$f(r, E) = \sqrt{\tilde{m}(r, E)/m}, \quad (12)$$

where $\tilde{m}(r, E)/m$ is the so-called momentum-dependent effective mass and is related to the LDOM Hartree-Fock potential as

$$\frac{\tilde{m}(r, E)}{m} = 1 - \frac{dV_{HF}(r, E)}{dE}. \quad (13)$$

Figure 3 also shows the Perey factor calculated with the widely used CH89 potential using Eq. (9) and assuming $\beta = 0.85$ fm. The Perey factors from LDOM and CH89 both have less effect in the surface region than the one calculated with NLDOM.

To calculate the $^{40}\text{Ca}(d,p)^{41}\text{Ca}$ cross sections a choice needs to be made for the optical potential U_p in the exit channel. In principle, this potential is auxiliary, and it is believed that choosing U_p that describes proton elastic scattering in the exit channel makes the remnant term $\sum_i V_{pi} - U_p$ in the transfer amplitude to disappear [1]. Since NLDOM was not fit to $p + ^{41}\text{Ca}$ scattering data, one choice for the auxiliary $p + ^{41}\text{Ca}$ potential U_p is to use NLDOM but evaluated with $A = 41$ instead of $A = 40$. An alternative, originally proposed in [24] and then further explored in [25], stems from the argument that the remnant term can be removed from the transition operator exactly, leading to a different model for the exit state wave function. In this model, the three-body Hamiltonian associated with the exit channel contains the p - ^{40}Ca optical potential, the n - ^{40}Ca bound-state potential, and no n - p interaction. In the limit of infinitely large core and in the zero-range approximation, the corresponding three-body wave function contains the p - ^{41}Ca distorted wave function calculated with the p - ^{40}Ca optical potential. Corrections due to recoil excitation and breakup are considered in [25]. For light nuclei the validity of the transfer amplitude with no remnant

has also been confirmed by [3]. We analyzed the (d, p) reaction with both choices for U_p , and the resulting cross sections were found to differ at the peak by about 1%. For the purposes of this study, both choices give practically the same result. Below, we choose to use NLDOM evaluated with $A = 41$ for U_p .

III. THE DEUTERON-TARGET POTENTIAL FOR (d, p) REACTIONS IN THE ADIABATIC APPROXIMATION

Following Johnson and Tandy [2] we retain only the first Weinberg component of the $A + n + p$ system in the (d, p) transfer amplitude since this amplitude is sensitive only to those parts of this wave function in which the neutron n is close to the proton p . Recently, exact continuum-discretized coupled channel calculations confirmed that this component indeed dominates [26]. The first Weinberg component is a product of the deuteron wave function $\phi_0(\mathbf{r})$ times the d - A relative motion wave function $\chi(\mathbf{R})$ which is the solution of the two-body Schrödinger equation with an adiabatic potential constructed from p - A and n - A optical potentials. The generalization of the deuteron adiabatic potential for the case of nonlocal, energy-independent N - A optical potentials of the Perey-Buck type is given in [7]. If nonlocal potentials (such as NLDOM) explicitly depend on energy then they should be evaluated at the energy $E = E_d/2 + \langle T_{np} \rangle_{V_{np}}/2$ and then treated as nonlocal and energy-independent [6]. The $\langle T_{np} \rangle_{V_{np}}/2$ term is half the n - p kinetic energy in deuteron averaged over the short-ranged potential V_{np} . The value of this term is about 57 MeV [6], so, for $E_d = 11.8$ MeV, the NLDOM potential should be evaluated at about 63 MeV. This at first sight seems counterintuitive. However, keeping in mind that neutron transfer takes place when proton and neutron in deuteron are at very short separations where the Heisenberg principle dictates high relative n - p momentum, it becomes clear that there is an additional kinetic energy in the N - A system which should be taken into account when choosing the energy at which the N - A potential should be evaluated.

A. Lowest order equivalent local model

The nonlocal Schrödinger equation for $\chi(\mathbf{R})$ from [7] can easily be generalized for the case of nonlocal optical potentials with multiple nonlocalities:

$$(T_R + U_C(R) - E_d)\chi(\mathbf{R}) = - \sum_{N=n,p} \sum_i \int ds dx \phi_1(\mathbf{x} + \alpha_1 \mathbf{s}) U_{NA,i} \left(\frac{\mathbf{x}}{2} - \mathbf{R} \right) \times H_i(s) \phi_0(\mathbf{x}) \chi \left(\frac{\alpha_2 \mathbf{s}}{2} + \mathbf{R} \right), \quad (14)$$

where \mathbf{R} is the radiusvector between d and A , T_R is the kinetic energy operator associated with \mathbf{R} , $\alpha_1 = A/(A+1)$, $\alpha_2 = (A+2)/(A+1)$, ϕ_0 is the deuteron ground state wave function, and

$$\phi_1(\mathbf{r}) = \frac{V_{np}(\mathbf{r})\phi_0(\mathbf{r})}{\langle \phi_0 | V_{np} | \phi_0 \rangle}. \quad (15)$$

Solving the nonlocal problem (14) directly is certainly possible, and was done recently in Ref. [27]. However, in this

paper, we construct the local-equivalent model, as simplified local-equivalent models can provide useful insight into the physics of a problem and make available transfer reaction codes applicable to nonlocal problems. The local-equivalent approximation of (14) can be obtained by expanding both $U_{NA,i}(\frac{\mathbf{x}}{2} - \mathbf{R})$ and $\chi(\frac{\alpha_2 \mathbf{s}}{2} + \mathbf{R})$ into Taylor series. In the lowest order approximation, using $U_{NA,i}(\frac{\mathbf{x}}{2} - \mathbf{R}) \approx U_{NA,i}(\mathbf{R})$ we get

$$(T_R + U_C(R) - E_d)\chi(\mathbf{R}) = - \sum_i U_{dA,i}(R) \tilde{H}_i^{(0)}(T_R) \chi(\mathbf{R}), \quad (16)$$

where $U_{dA,i}(R) = U_{nA,i}(R) + U_{pA,i}(R)$,

$$\tilde{H}_i^{(0)}(T_R) = M_{0,i}^{(0)} \sum_{n=0}^{\infty} \frac{(-)^n}{n!} \left(\frac{\mu_d \alpha_2^2}{2\hbar^2} (\beta_{n,i}^{(0)})^2 T_R \right)^n, \quad (17)$$

the coefficients $\beta_{n,i}^{(0)}$ are defined by

$$\beta_{n,i}^{(0)} = \frac{1}{\sqrt{2}} \left[\frac{M_{2n,i}^{(0)}}{(2n+1)!! M_{0,i}^{(0)}} \right]^{\frac{1}{2n}}, \quad (18)$$

and the moments $M_{2n,i}^{(0)}$ are defined by

$$M_{2n,i}^{(0)} = \int ds dx s^{2n} H_i(s) \phi_1(\mathbf{x} - \alpha_1 \mathbf{s}) \phi_0(\mathbf{x}). \quad (19)$$

Equation (16) is further simplified by introducing the local-energy approximation [1],

$$T_R \approx T_0(R) = E_d - U_{loc}^0(R) - U_C(R), \quad (20)$$

where the local potential $U_{loc}^0(R)$ is defined as

$$U_{loc}^0(R) = \sum_i U_{dA,i}(R) \tilde{H}_i^{(0)}(T_0(R)). \quad (21)$$

This approximation works very well for nucleon optical potentials with one nonlocality parameter [7]. We will show that it remains good for NLDOM with its multiple nonlocalities, but we first present the results of calculations of $U_{loc}^0(R)$ for $E_d = 11.8$ MeV using the deuteron wave function from the Hultén model, the same as in [7]. It is pointed out in [7] that a realistic deuteron wave function gives the moment $M_0^{(0)}$ which is very similar to that obtained with the Hultén wave function. In Table III we show the calculated $\beta_{n,i}^{(0)}$ and $M_{0,i}^{(0)}$ terms. For very small nonlocalities, $\beta_{n,i}^{(0)}$ should be approximately equal to $\beta_i/2$ [7,28]. For typical nonlocalities of $\sim 0.8 - 1.0$ fm they are $\sim 10\%$ smaller than the $\beta_i/2$ value but are essentially independent of n , allowing one to replace the $\beta_{n,i}^{(0)}$ coefficients with a constant. We define this constant to be

$$\beta_{d,i} = \beta_{1,i}^{(0)}. \quad (22)$$

The summation in (17) then gives $\tilde{H}_i^{(0)}(T_R)$ an exponential form

$$\tilde{H}_i^{(0)}(T_R) \approx \mathcal{H}_i^{(0)}(\gamma_i T_R) = M_{0,i}^{(0)} \exp(-\gamma_i T_R), \quad (23)$$

where

$$\gamma_i = \frac{\mu_d \alpha_2^2 \beta_{d,i}^2}{2\hbar^2}. \quad (24)$$

TABLE III. Coefficients $\beta_n^{(\lambda)}$ (in fm) and moments $M_0^{(\lambda)}$ (in fm^{2 λ}) for $\lambda = 0, 1$ and for six different values of the nucleon nonlocality β that are used in the NLDOM.

n	$\beta = 0.64$ fm	$\beta = 0.84$ fm	$\beta = 0.94$ fm	$\beta = 1.04$ fm	$\beta = 1.55$ fm	$\beta = 2.07$ fm
$\beta_1^{(0)}$	0.3075	0.3932	0.4393	0.4802	0.6821	0.8679
$\beta_2^{(0)}$	0.3082	0.3947	0.4414	0.4829	0.6895	0.8824
$\beta_3^{(0)}$	0.3088	0.3960	0.4431	0.4851	0.6955	0.8938
$\beta_4^{(0)}$	0.3093	0.3970	0.4445	0.4869	0.7004	0.9031
$\beta_5^{(0)}$	0.3097	0.3979	0.4457	0.4885	0.7045	0.9108
$\beta_6^{(0)}$	0.3101	0.3986	0.4468	0.4898	0.7080	0.9174
$\beta_7^{(0)}$	0.3104	0.3993	0.4477	0.4910	0.7111	0.9231
$\beta_8^{(0)}$	0.3107	0.3999	0.4486	0.4921	0.7139	0.9281
$M_0^{(0)}$	0.855	0.791	0.756	0.726	0.580	0.464
$\beta_1^{(1)}$	0.3100	0.3981	0.4459	0.4885	0.7030	0.9062
$\beta_2^{(1)}$	0.3104	0.3991	0.4473	0.4903	0.7077	0.9151
$\beta_3^{(1)}$	0.3108	0.3999	0.4484	0.4917	0.7115	0.9224
$\beta_4^{(1)}$	0.3111	0.4006	0.4494	0.4930	0.7148	0.9286
$\beta_5^{(1)}$	0.3115	0.4013	0.4502	0.4941	0.7177	0.9339
$\beta_6^{(1)}$	0.3118	0.4018	0.4510	0.4951	0.7202	0.9384
$\beta_7^{(1)}$	0.3120	0.4023	0.4517	0.4959	0.7224	0.9424
$\beta_8^{(1)}$	0.3122	0.4028	0.4523	0.4967	0.7243	0.9459
$M_0^{(1)}$	0.098	0.149	0.179	0.206	0.341	0.451

As β_i increases beyond 1.0 fm, the approximation in Eq. (22) becomes less valid and the coefficients $\beta_{n,i}^{(0)}$ deviate from $\beta_i/2$ even more. This trend can be seen in Table III and is especially apparent for $\beta = 2.07$ fm, which is the largest nonlocality parameter used in NLDOM. Thus, we solve Eqs. (17), (20), and (21) by restricting the sum over n in (17) by some n_{\max} . We found that $n_{\max} = 6$ is sufficient to obtain a converged solution for U_{loc} . However, we also found that using Eq. (22) leads to practically the same result because the real and imaginary parts of the NLDOM terms associated with $\beta = 2.07$ fm are small at the energies being considered. The U_{loc} potentials obtained from solution of (21) with (17) and (23) are shown in Fig. 4. Using Eq. (22) for all nonlocality parameters, one obtains U_{loc} from the transcendental equation

$$U_{\text{loc}}^0 = \sum_i M_{0,i}^{(0)} U_{dA,i} \times \exp \left[-\frac{\mu_d \alpha_2^2 \beta_{d,i}^2}{2\hbar^2} (E_d - U_{\text{loc}}^0 - U_C) \right]. \quad (25)$$

The Coulomb potential U_C is approximated by a constant, given by

$$U_C = -1.08 + \frac{1.35Z}{A^{1/3}}, \quad (26)$$

which was used in Refs. [8,29]. The difference between using this approximation and a more realistic potential is only about 1%, in terms of the peak cross section of the proton angular distribution for the $^{40}\text{Ca}(d, p)^{41}\text{Ca}$ reaction at $E_d = 11.8$ MeV.

B. Correction to the local-energy approximation in the lowest order

It was shown in [7] that corrections to the lowest order local model beyond the local-energy approximation are small because they are the fourth-order effect of the nucleon nonlocality β , as the second-order terms cancel each other for Perey-Buck potentials with one nonlocality parameter. The NLDOM from [9] contains several nonlocalities, and second-order contributions may not cancel. Moreover, some of these nonlocalities are large so that the contributions beyond the local-energy approximation are expected to be larger than

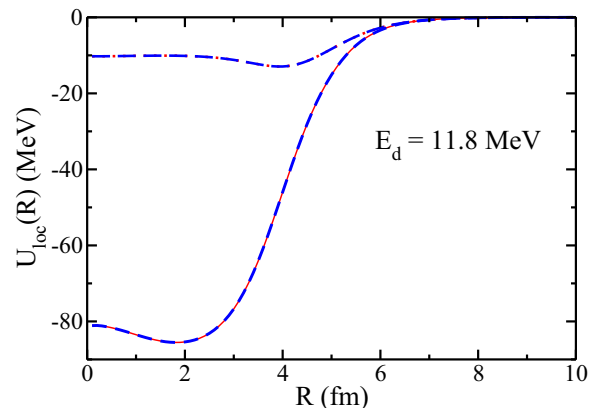


FIG. 4. Real and imaginary parts of the local-equivalent NLDOM potential calculated using the exponential form (solid and dotted lines, respectively) and using the series form (thick short-dashed and long-dashed lines, respectively) with $n_{\max} = 6$.

those in [7]. In this section we study these corrections using results from Secs. IV.C and A.4 of [7]. Including leading correction term, linear in the kinetic energy operator T_R , and using the exponential form (23) for $\tilde{H}_i^{(0)}(T_R)$, the right-hand side of Eq. (16) becomes

$$\begin{aligned} & \sum_i U_{dA,i} \mathcal{H}_i^{(0)}(\gamma_i T_R) \chi(\mathbf{R}) \\ & \approx \sum_i U_{dA,i} \mathcal{H}_i^{(0)}(\gamma_i T_0) \left[1 - \gamma_i (T_R - T_0 + \Delta_i) \right. \\ & \quad \left. - \frac{\hbar^2 \gamma_i^2}{2\mu_d} \nabla T_0 \cdot \nabla_R \right] \chi(\mathbf{R}), \end{aligned} \quad (27)$$

where the energy correction Δ_i , arising because T_R and T_0 do not commute, is given by

$$\Delta_i = \frac{\hbar^2 \gamma_i}{2\mu_d} \left(\frac{T_0''}{2} + \frac{T_0'}{R} - \frac{\gamma_i}{3} T_0'^2 \right). \quad (28)$$

The solution of Eq. (16) in this approximation is the product

$$\chi(\mathbf{R}) = f_0(\mathbf{R}) \varphi(\mathbf{R}), \quad (29)$$

where φ is the scattering wave of the local model

$$(T_R + U_C - E_d) \varphi = -(U_{\text{loc}}^0 + \Delta U_0) \varphi. \quad (30)$$

The U_{loc}^0 term is discussed in the previous section, and the correction term ΔU_0 is

$$\Delta U_0 = \frac{T_R f_0}{f_0} + \frac{\hbar^2}{4\mu_d} \left(\frac{U_2 T_0'}{1 - U_1} \right)^2 - \frac{U_\Delta}{1 - U_1} \quad (31)$$

with

$$U_n(R) = \sum_i U_{dA,i} \mathcal{H}_i^{(0)}(\gamma_i T_0) \gamma_i^n, \quad (32)$$

$$U_\Delta(R) = \sum_i U_{dA,i} \mathcal{H}_i^{(0)}(\gamma_i T_0) \gamma_i \Delta_i. \quad (33)$$

The function f_0 is the analog of the Perey factor discussed in Sec. II. It modifies the scattering wave function $\varphi(\mathbf{R})$ in the nuclear interior and satisfies the first-order differential equation

$$\frac{\nabla f_0}{f_0} = -\frac{1}{2} \frac{U_2(R)}{1 - U_1(R)} \nabla T_0, \quad (34)$$

with the boundary condition $f(R) \rightarrow 1$ at $R \rightarrow \infty$. The solution of this equation is

$$f_0(R) = \exp \left(\frac{1}{2} \int_R^\infty dR_1 \frac{U_2(R_1)}{1 - U_1(R_1)} T_0'(R_1) \right). \quad (35)$$

Because of multiple nonlocalities, the analytical integration in (35) cannot be done. So, it is difficult to see if the contributions to f_0 from second-order terms on $\beta_{d,i}$ cancel. Most likely, they do not.

The Perey factor f_0 and the correction ΔU_0 to the equivalent local potential U_{loc}^0 are shown in Figs. 5 and 6, respectively, for $d + {}^{40}\text{Ca}$ at deuteron incident energy of 11.8 MeV. The Perey factor increases the scattering wave in the nuclear interior by about 6%, which is a couple of percent higher than the result in

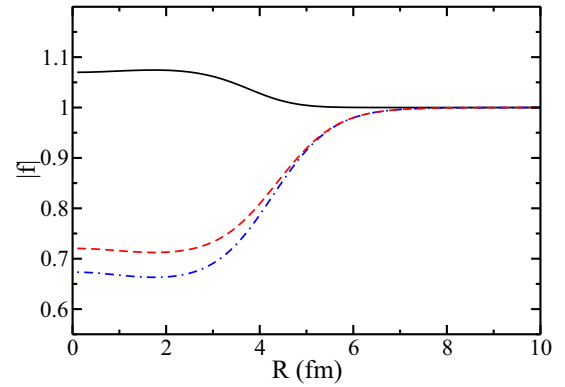


FIG. 5. Perey factors f_0 (solid), f_1 (dot-dashed), and f (dashed) calculated with NLDOM for $E_d = 11.8$ MeV.

[7]. The correction to U_{loc}^0 , however, remains small. Its real part is very close to the one obtained in [7] in the maximum, being about 150 keV, while the imaginary part is much smaller. Thus, for NLDOM the second-order corrections most likely remain small and the local-energy approximation remains good.

C. First-order corrections

The first order correction to the local-equivalent lowest-order model of Sec. III A is obtained by retaining two terms in the Taylor series expansion of the central potential

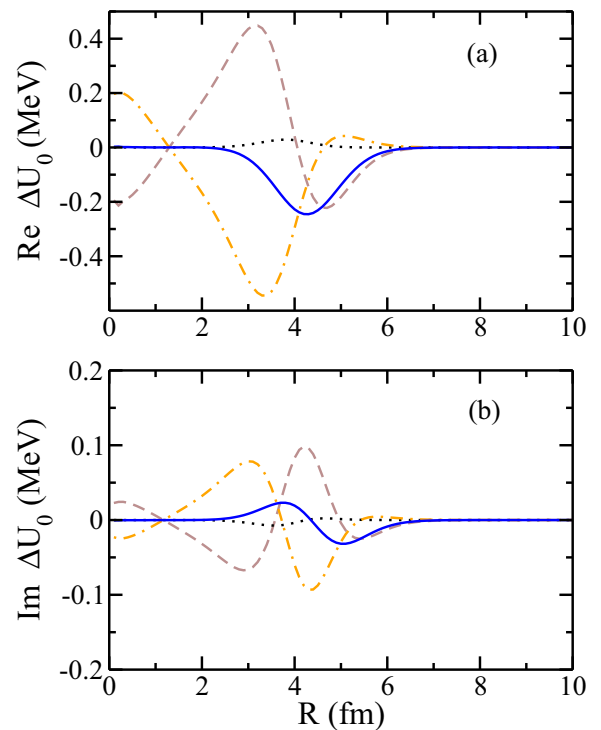


FIG. 6. (a) The real parts and (b) the imaginary parts of ΔU_0 (solid) and the first (dashed), second (dotted), and third (dot-dashed) terms in Eq. (31).

$U_{NA}(\pm \frac{x}{2} - \mathbf{R})$:

$$U\left(\pm \frac{\mathbf{x}}{2} - \mathbf{R}\right) \approx U(\mathbf{R}) \mp \frac{1}{2} \mathbf{x} \cdot \nabla U(\mathbf{R}). \quad (36)$$

In this case, using techniques of [7], we obtain the following:

$$\begin{aligned} & (T_R + U_C(R) - E_d)\chi(\mathbf{R}) \\ &= - \sum_i U_{dA,i}(R) \mathcal{H}_i^{(0)}(\gamma_i T_R) \chi(\mathbf{R}) \\ & \quad - \sum_i \nabla [U_{dA,i}(R)] \mathcal{H}_i^{(1)}(\tilde{\gamma}_i T_R) \nabla \chi(\mathbf{R}), \end{aligned} \quad (37)$$

where

$$\mathcal{H}_i^{(1)}(\tilde{\gamma}_i T_R) = \frac{M_{0,i}^{(1)}}{3M_{0,i}^{(0)}} \mathcal{H}_i^{(0)}(\tilde{\gamma}_i T_R) \quad (38)$$

and the moments $M_{2n,i}^{(1)}$ are defined as

$$M_{2n,i}^{(1)} = \int ds d\mathbf{x} s^{2n} H_i(s) \phi_1(\mathbf{x} - \alpha_1 s) \phi_0(\mathbf{x}) \frac{\alpha_2 s \cdot \mathbf{x}}{4}. \quad (39)$$

The new factor $\tilde{\gamma}_i$ arises from the fact that the moments $M_{2n,i}^{(1)}$ lead to new coefficients $\beta_{n,i}^{(1)}$ that are also practically independent of n (see Table III). Introducing a new constant

$$\tilde{\beta}_{d,i} = \beta_{1,i}^{(1)}, \quad (40)$$

the factor $\tilde{\gamma}_i$ can be written as

$$\tilde{\gamma}_i = \frac{\mu_d \alpha_2 \tilde{\beta}_{d,i}^2}{2\hbar^2}. \quad (41)$$

The coefficients $\beta_{n,i}^{(1)}$ are defined as

$$\beta_{n,i}^{(1)} = \frac{1}{\sqrt{2}} \left[\frac{3M_{2n,i}^{(1)}}{(2n+3)!! M_{0,i}^{(1)}} \right]^{\frac{1}{2n}}. \quad (42)$$

At this point we make the local-energy approximation (20) but we also include the correction to this approximation similar to that considered above. We expand $\mathcal{H}_i^{(0)}(\gamma_i T_R)$ in the first term of right-hand side of Eq. (37) as in Eq. (27), but we use a simpler expansion for $\mathcal{H}_i^{(1)}(\tilde{\gamma}_i T_R)$ in the second term,

$$\mathcal{H}_i^{(1)}(\tilde{\gamma}_i T_R) = \mathcal{H}_i^{(1)}(\tilde{\gamma}_i T_0) [1 - \tilde{\gamma}_i (T_R - T_0)], \quad (43)$$

because $\mathcal{H}_i^{(1)}(\tilde{\gamma}_i T_R)$ is an order of magnitude smaller than $\mathcal{H}_i^{(0)}(\gamma_i T_R)$ so that the higher order terms on $\tilde{\beta}_{d,i}$ in terms with Δ_i and $\nabla \cdot \nabla_R$ will be small. For a similar reason we keep only the leading correction to $(T_R - T_0) \nabla \chi(\mathbf{R})$:

$$(T_R - T_0) \nabla \chi(\mathbf{R}) \approx \nabla T_0 \chi(\mathbf{R}). \quad (44)$$

With these approximations we can solve Eq. (37) by introducing the same representation $\chi(\mathbf{R}) = f(\mathbf{R})\varphi(\mathbf{R})$ used both for proton scattering in Sec. II and for correction to local-energy-approximation above. The scattering wave φ is found from the local equation

$$(T_R + U_C - E_d)\varphi = -(U_{\text{loc}}^0 + \Delta U)\varphi, \quad (45)$$

with the same U_{loc} as before but corrected by

$$\Delta U = \Delta U_0 + \Delta U_1, \quad (46)$$

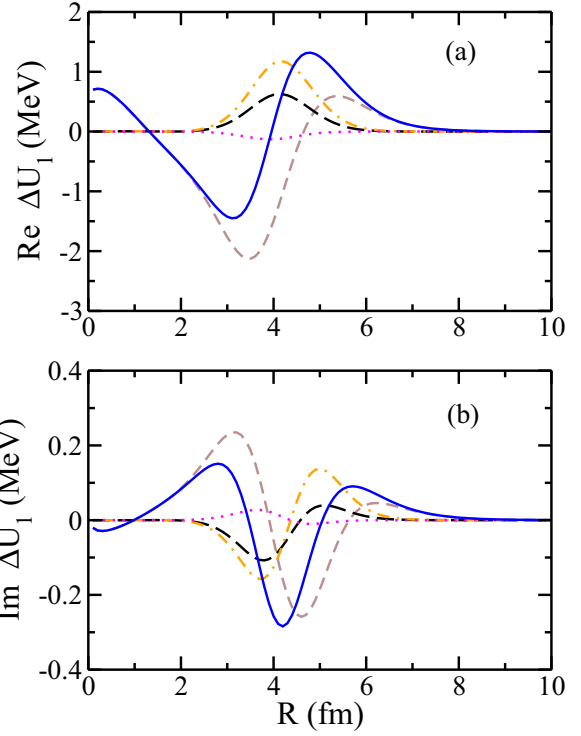


FIG. 7. (a) The real parts and (b) the imaginary parts of ΔU_1 (solid) and the first (short-dashed), second (long-dashed), third (dot-dashed), and fourth (dotted) terms in Eq. (47).

in which the first term is the same as in Eq. (31), and the second term is given by

$$\Delta U_1 = \frac{T_R f_1}{f_1} + \frac{\mu_d}{\hbar^2} \frac{U_0^2}{(1-U_1)^2} - \frac{U_1 T_0'}{1-U_1} - \frac{1}{2} \frac{U_0 U_2 T_0'}{(1-U_1)^2}, \quad (47)$$

where

$$U_n(R) = \sum_i \nabla [U_{dA,i}(R)] \mathcal{H}_i^{(1)}(\tilde{\gamma}_i T_0) \tilde{\gamma}_i^n. \quad (48)$$

The Perey factor f is the solution of the first-order differential equation

$$\frac{\nabla f}{f} = \frac{\mu_d}{\hbar^2} \frac{U_0}{1-U_1} - \frac{1}{2} \frac{U_2 T_0'}{1-U_1} \quad (49)$$

with the boundary condition $f(R) \rightarrow 1$ at $R \rightarrow \infty$. The solution to this equation can be written as

$$f(R) = f_0(R) f_1(R) \quad (50)$$

where f_0 is given by Eq. (35) and f_1 is given by

$$f_1(R) = \exp\left(-\frac{\mu_d}{\hbar^2} \int_R^\infty dR' \frac{U_0(R')}{1-U_1(R')}\right). \quad (51)$$

The correction ΔU_1 and the four terms on the right-hand side of Eq. (47) are shown in Fig. 7. The Perey factors f_1 and f are plotted in Fig. 5. The correction ΔU_1 and the Perey factor f are comparable to the corresponding quantities obtained in [7] for a Perey-Buck potential with a single nonlocality. We can rewrite this factor in the form of Eq. (10). The corresponding

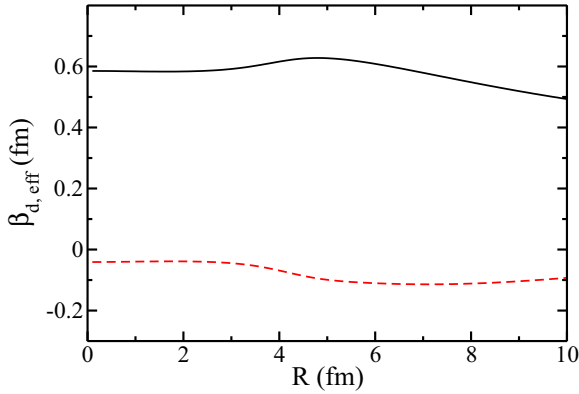


FIG. 8. Real part (solid) and imaginary part (dashed) of effective deuteron nonlocality as a function of r for $E_d = 11.8$ MeV.

effective deuteron nonlocality, $\beta_{d,\text{eff}}$ is plotted in Fig. 8 as a function of r for $E_d = 11.8$ MeV. Note that $\beta_{d,\text{eff}}$ is complex, but, as in the case for protons, the imaginary part is small and changes the cross section of the proton angular distribution by less than 0.5%. The real part lies between 0.50 and 0.60 fm, and these values are very similar to 0.56 fm, which is the value used for deuteron elastic scattering.

IV. TRANSFER REACTION $^{40}\text{Ca}(d, p)^{41}\text{Ca}$ AT 11.8 MeV

We calculated the proton angular distributions for the $^{40}\text{Ca}(d, p)^{41}\text{Ca}$ reaction at $E_d = 11.8$ MeV in the adiabatic zero-range approximation. The finite range effects at these energies are expected to be small [30]. The standard value for D_0 , given by $D_0^2 = 15615 \text{ MeV}^2 \text{ fm}^3$, was used. The distorted potentials both in the deuteron and proton channels, generated with NLDOM, were read into the TWOFNR code [31]. There is no option in TWOFNR for incorporating complex r -dependent effective nonlocalities $\beta_{\text{eff}}(r)$. Therefore, in order to reduce the corresponding distorted waves in the nuclear interior, we multiplied the NLDOM $\langle ^{40}\text{Ca} | ^{41}\text{Ca} \rangle$ overlap function (also read into the TWOFNR code) by the Perey factors of the proton and deuteron channels, given by Eqs. (10) and (50), respectively. This is legitimate in the zero-range approximation, where the integrand of the (d, p) reaction amplitude is a function of only one vector variable. In this case, the Perey factor for the proton channel had to be calculated on a different grid.

The overlap function $I_{\text{DOM}}^{\text{NL}}(r)$, generated by NLDOM and read into TWOFNR, is compared in Fig. 9 to (i) the overlap function $I_{\text{WS}}(r)$ obtained from a Woods-Saxon potential with standard geometry ($r_0 = 1.25$ fm, $a = 0.65$ fm); (ii) the overlap function $I_{\text{DOM}}^{\text{L}}(r)$ generated with LDOM; and (iii) the overlap function $I_{\text{WS}}^{\text{NL}}(r)$, calculated in a standard Woods-Saxon model employing a nonlocality correction via the Perey factor with $\beta = 0.85$ fm. All these overlap functions are normalized to 0.73, which is the spectroscopic factor calculated from NLDOM.

We have found that $I_{\text{DOM}}^{\text{NL}}(r)$ can be described very well (with about 1% accuracy) by a local two-body Woods-Saxon potential model that has the radius $r_0 = 1.252$ fm, diffuseness $a = 0.718$ fm and the spin-orbit strength $V_{s.o.} = 6.25$ MeV.

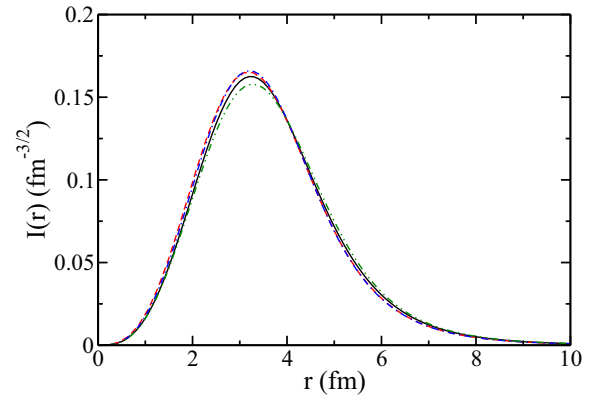


FIG. 9. Overlap functions calculated using NLDOM (solid), LDOM (dashed), a Woods-Saxon potential with standard geometry (dot-dashed), and a Woods-Saxon potential but corrected with a Perey factor with $\beta = 0.85$ fm (dot-dot-dashed).

These parameters are very close to the standard values of $r_0 = 1.25$ fm and $a = 0.65$ fm used to generate $I_{\text{WS}}(r)$. However, relative to $I_{\text{WS}}(r)$, using $I_{\text{DOM}}^{\text{NL}}(r)$ as the overlap function increases the transfer cross section at the peak, $\sigma_{d,p}^{\text{peak}}$, by about 15% (for the reaction at $E_d = 11.8$ MeV).

The NLDOM and LDOM overlap functions have similar shapes, but their r.m.s. radii and asymptotic normalization coefficients (ANCs) somewhat differ. The $I_{\text{DOM}}^{\text{NL}}(r)$ radius of 4.030 fm is slightly larger than that of $I_{\text{DOM}}^{\text{L}}(r)$, which is 3.965 fm. Also, the single-particle ANC b_{lj} for $I_{\text{DOM}}^{\text{NL}}(r)$ is $2.48 \text{ fm}^{-1/2}$, which is about 10% larger than that of $I_{\text{DOM}}^{\text{L}}(r)$. The spectroscopic factors for these two overlaps are practically the same. As a result, $I_{\text{DOM}}^{\text{NL}}(r)$ produces a larger many-body ANC squared, $C_{lj}^2 = S_{lj} b_{lj}^2$, equal to 4.5 fm^{-1} , whereas $I_{\text{DOM}}^{\text{L}}(r)$ has $C_{lj}^2 = 3.8 \text{ fm}^{-1}$. Interestingly, the NLDOM value of C_{lj}^2 is very close to the prediction of $C_{lj}^2 = 4.4 \text{ fm}^{-1}$ of the source term approach [32], which is based on the independent-particle-model for ^{40}Ca and ^{41}Ca . This approach accounts for correlations between nucleons via an effective interaction potential of the removed nucleon with nucleons in the core [33].

The standard overlap $I_{\text{WS}}(r)$ is very close to $I_{\text{DOM}}^{\text{L}}(r)$ (see Fig. 9). The overlap $I_{\text{WS}}^{\text{NL}}(r)$, which is sometimes used in (d, p) calculations, has a distinctly larger radius and is not consistent with NLDOM. Below, in all our (d, p) calculations we use only the NLDOM overlap with its own normalization of 0.73, which allows for making conclusions from comparison between theoretical and experimental cross sections without any further renormalization.

Proton angular distributions calculated using the NLDOM potentials are presented in Fig. 10. The solid curve corresponds to the lowest-order result. The long-dashed curve shows that incorporating the first-order corrections for the proton channel, via Eqs. (5) and (10), reduces the lowest-order (d, p) peak cross sections $\sigma_{d,p}^{\text{peak}}$ by 3%. Further first-order corrections, coming from Eqs. (46) and (50) for the deuteron channel and shown by the short-dashed curve, reduces $\sigma_{d,p}^{\text{peak}}$ by another 5%.

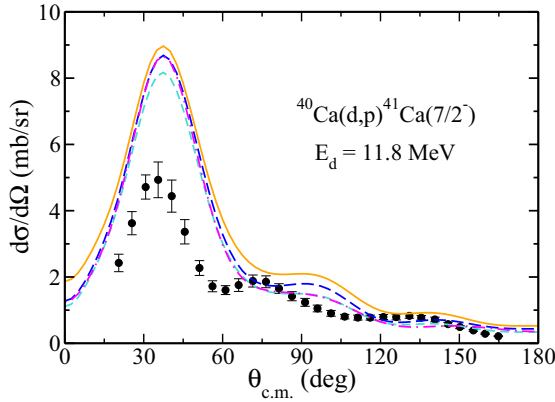


FIG. 10. The differential $^{40}\text{Ca}(d,p)^{41}\text{Ca}(7/2^-)$ cross sections with $E_d = 11.8$ MeV generated using NLDOM without the corrections from Eqs. (5), (10) and Eqs. (46), (50) (solid), with the corrections for the proton channel (long-dashed), with the corrections for both the proton and deuteron channels (short-dashed), and with the spin-orbit potential in addition to the other corrections (dot-dashed). The experimental data are also shown (dots).

Finally, including the spin-orbit potential raises $\sigma_{d,p}^{\text{peak}}$ and makes it comparable to the cross sections obtained with no corrections in the deuteron channel (the dot-dashed curve). The experimental data are from [34]. The spread between all these calculations does not exceed 12% and all of them considerably overestimate the experimental data, shown in Fig. 10 as well. This overestimation (by about 70% after normalizing overlap function to 0.73) cannot come from the local approximations we have made to solve the nonlocal problem. The first-order corrections of about 12% mean that the second-order corrections would most likely be around 1% or less. Thus, other reasons for this overestimation should be investigated.

It was already noted in [7,28] that the adiabatic model with nonlocal energy-independent potentials gives higher cross sections, as compared to the standard adiabatic model, due to a weaker attraction in the deuteron channel. The higher cross sections are confirmed in other (d,p) studies with such potentials [27]. Here, the overestimation of the (d,p) cross sections using the NLDOM is stronger than in the case of energy-independent potentials. This can be seen in Fig. 11, which compares the NLDOM angular distribution with the angular distributions from two nonlocal, energy-independent potentials, referred to as GR [29] and TPM [35]. Figure 11 also shows the angular distribution from another nonlocal, energy-dependent potential, referred to as GRZ [8] and used previously in [6]. This potential generates an angular distribution very similar to the one generated with NLDOM. The structure of the GRZ potential is not as complicated as the NLDOM potential, but it has a typical low-energy behavior of the imaginary part, vanishing at $E \rightarrow 0$ (for $N = Z$). For all distributions, the corresponding nucleon optical model parametrizations were consistently used to calculate the exit and entrance channel potentials, taking into account the first-order corrections and the Perey effect.

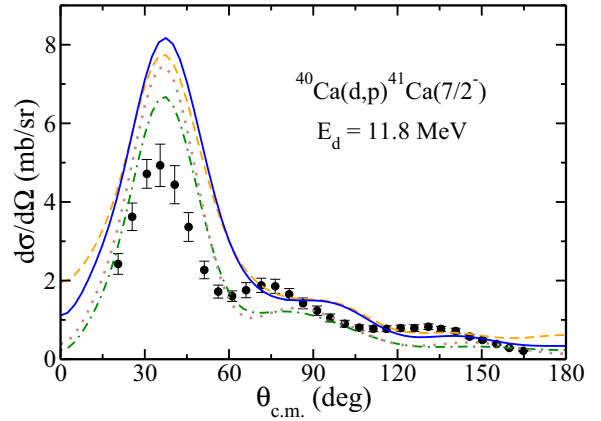


FIG. 11. The differential $^{40}\text{Ca}(d,p)^{41}\text{Ca}(7/2^-)$ cross sections with $E_d = 11.8$ MeV generated using the NLDOM (solid), GRZ (dashed), GR (dot-dashed), and TPM (dotted) nonlocal parametrizations.

To understand the $\sim 20\%$ difference in $\sigma_{d,p}^{\text{peak}}$ shown in Fig. 11, we compare the entrance and exit channel potentials generated from the four nonlocal parametrizations and present them in Fig. 12. The NLDOM, GRZ, and GR generate real parts of similar depths and sizes both in entrance and exit channels while the TPM produces a real part of a moderately larger radial extent. The imaginary parts, however, show a marked difference, in both the entrance and exit channels. The energy-independent parametrizations GR and TPM produce a much larger imaginary part in the surface region than the energy-dependent parametrizations NLDOM and GRZ. The smaller imaginary parts produce less absorption thus increasing $\sigma_{d,p}^{\text{peak}}$. This is even better seen in Fig. 13, which shows the (d,p) angular distributions calculated with four different parametrizations for the exit proton channel and using NLDOM for the deuteron channel. In this figure, we have also added the calculations with LDOM [21] and the widely used local CH89 [36] parametrizations in the proton channel while keeping the NLDOM in the deuteron channel. The LDOM and CH89 proton potentials are shown in panels (c) and (d) of Fig. 12.

Figure 13 shows that predictions with NLDOM, LDOM and GRZ form a different class from those obtained with GR, TPM, and CH89. All the potentials from the first class have smaller imaginary parts and/or volume integrals than the potentials from the second class. Thus, overestimation of the cross section calculated with NLDOM seems to be at least partly due to a weaker absorption in the exit channel potential.

The weaker absorption may not be the only reason for large cross sections obtained with NLDOM. It was discussed in detail in [37] that a particular relation between optical potentials in entrance and exit channels results in destructive interference between the ingoing and outgoing partial waves leading to l localization of radial (d,p) amplitudes in the adiabatic model. A similar situation may occur here. Indeed, the standard adiabatic Johnson-Soper (JS) [38] calculations using both the local-equivalent NLDOM and LDOM potentials, taken at $E = E_d/2$, predict much lower cross sections (see Fig. 14) while the imaginary parts of the Johnson-Soper

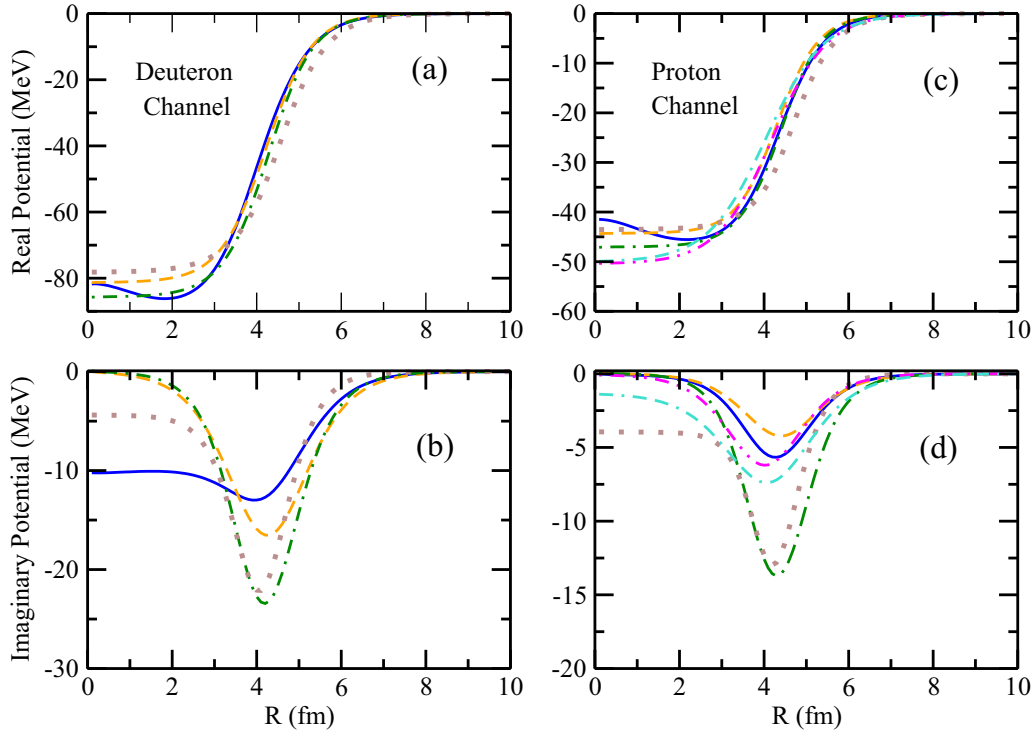


FIG. 12. Panels (a) and (b) show the real and imaginary parts of the entrance channel potentials for the NLDOM (solid), GRZ (dashed), GR (dot-dashed), and TPM (dotted) nonlocal parametrizations used in Fig. 11, while panels (c) and (d) show these quantities for the exit channel. Panels (c) and (d) also show the potentials calculated using LDOM (dot-dot-dashed) and CH89 (dash-dash-dotted).

potentials, shown in Fig. 15, are much smaller than those of local-equivalent deuteron potentials obtained in this work (TJ). This could be an indication of constructive interference between the ingoing and outgoing partial waves generated with NLDOM potentials. A new procedure was proposed in Sec. VI B of Ref. [6], explaining how phenomenological local energy-dependent optical potentials can be used in (d, p) calculations if they represent local equivalents of nonlocal

potentials. Using the LDOM potential within this procedure and assuming a hidden nonlocality of 0.85 fm gives very similar results to NLDOM both for the real part of deuteron distorting potential (Fig. 15) and the (d, p) cross sections (Fig. 14) despite stronger imaginary part in the deuteron

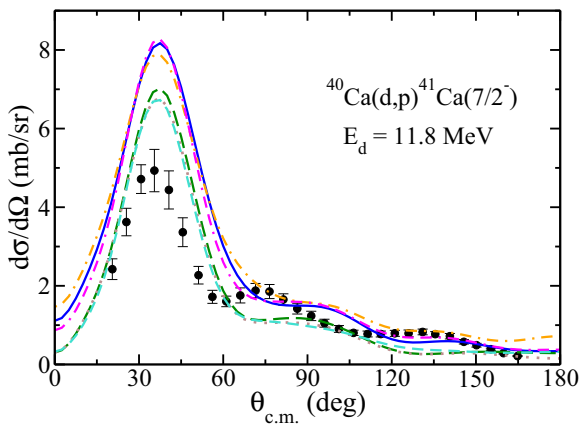


FIG. 13. The differential $^{40}\text{Ca}(d, p)^{41}\text{Ca}(7/2^-)$ cross sections with $E_d = 11.8$ MeV generated using NLDOM for the entrance channel and the overlap function and using NLDOM (solid), GRZ (dot-dashed), GR (long-dashed), TPM (dotted), LDOM (dash-dash-dotted), and CH89 (short-dashed) for the exit channel.

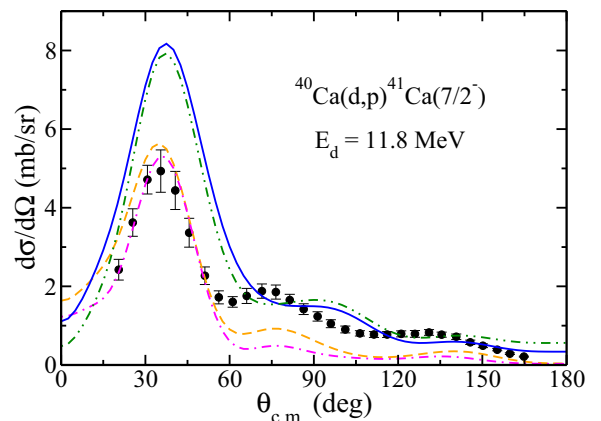


FIG. 14. The differential $^{40}\text{Ca}(d, p)^{41}\text{Ca}(7/2^-)$ cross sections with $E_d = 11.8$ MeV calculated with NLDOM (solid) and LDOM (dot-dot-dashed) using the TJ prescription, which evaluates the optical potentials at the shifted energy $E = E_d/2 + 57$ MeV. Also shown are the results from using the JS prescription, which evaluates the optical potentials at the usual energy $E = E_d/2$, with both NLDOM (dashed) and LDOM (dot-dashed).

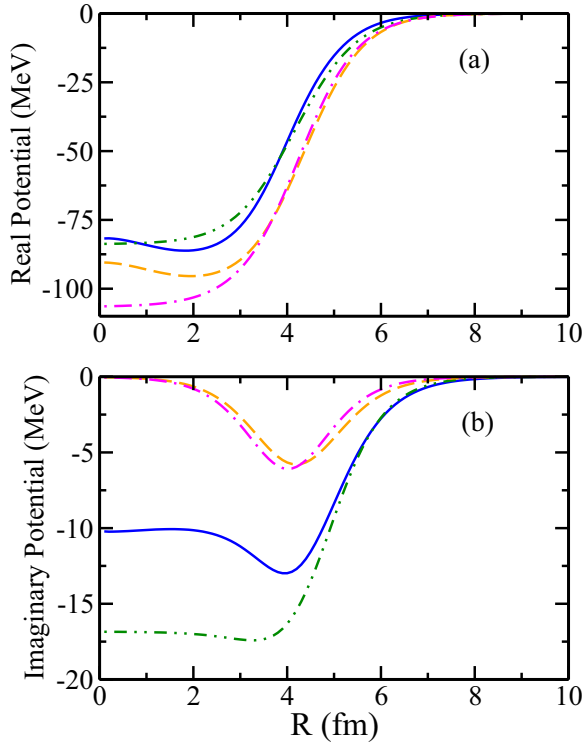


FIG. 15. (a) Real and (b) imaginary parts of the deuteron potential for the $^{40}\text{Ca}(d,p)^{41}\text{Ca}(7/2^-)$ reaction at $E_d = 11.8$ MeV calculated with NLDOM (solid) and LDOM (dot-dot-dashed) using the TJ prescription, which evaluates the optical potentials at the shifted energy $E = E_d/2 + 57$ MeV. Also shown are the results from using the JS prescription, which evaluates the optical potentials at the usual energy $E = E_d/2$, with both NLDOM (dashed) and LDOM (dot-dashed).

channel. Although the Johnson-Soper cross sections are close to experimental data, in light of recent findings [6,7,27,28], constructing the adiabatic potentials from nucleon optical potentials taken at half the deuteron incident energy does not seem to be justified anymore.

V. CONCLUSION

We presented the first adiabatic (d,p) calculations with the NLDOM potential, which has been designed with the aim of forging the link between nuclear structure and nuclear reactions in a consistent way. It has its roots in the underlying self-consistent Green's functions theory and possesses the fundamental properties—nonlocality, energy-dependence, and dispersion relations—that arise from the complex structure of the target. The NLDOM explicitly takes into account a number of components of nuclear many-body theory that many other optical models do not.

One could expect that using an advanced optical potential parametrization such as NLDOM would result in properly fixed single-nucleon properties both below and above the Fermi surface crucial for agreement between predictions of (d,p) reaction theory and experimental data. However, we have shown that using the NLDOM to generate the distorting potentials entering the (d,p) amplitude strongly overestimates

the (d,p) cross sections despite the reduced strength of the NLDOM one-neutron overlap function employed in the calculations. Moreover, the NLDOM predictions are very similar to those made with a much simpler nonlocal potential GRZ derived within Watson multiple scattering theory and Wolfenstein's parametrization of the nucleon-nucleon scattering amplitude [8,29]. The energy dependence is presented in GRZ only in the imaginary part.

Since we do not have strong reason to doubt the quality of the NLDOM parametrization the main assumptions of the (d,p) theory used in the present calculations should be reviewed. We list them below:

- (1) The (d,p) amplitude contains a projection of the total many-body wave function into the three-body channel $A + n + p$ only. Projections onto all excited states of A are neglected.
- (2) Only n - A and p - A potentials are used to calculate the $A + n + p$ projection. According to [6] there are also multiple scattering terms playing the role of a three-body $A + n + p$ force. These are neglected.
- (3) Averaged n - A and p - A potentials were obtained using the procedure from Ref. [6], which uses the adiabatic approximation. Corrections to this approximation may change the energy value at which these potentials should be evaluated.
- (4) It was assumed that the (d,p) transition operator contains the V_{np} term only. Any other terms present in this amplitude [1] are neglected.
- (5) It was shown in [25] that keeping V_{np} only in the (d,p) transition operator modifies the proton channel wave function. In our particular case, this would result in using the p - ^{40}Ca optical potential in the $p + ^{41}\text{Ca}$ channel. We have not seen any difference in (d,p) cross sections when replacing ^{41}Ca by ^{40}Ca and this could mean that the averaging procedure, introduced in [6], when applied to the special $A + n + p$ three-body model, that does not have V_{np} and has different asymptotic conditions [25], may result in completely different requirements to the proton distorting potential in the exit channel. Using proton optical potentials may not be justified anymore.
- (6) We used the adiabatic approximation to solve the three-body Schrödinger equation.

The deviation from the adiabatic approximation for solving the Schrödinger equation has been studied both within the continuum-discretized coupled channel method [3] and using Faddeev equations [39]. Although these corrections can be non-negligible, they cannot be responsible for 70% overestimation of (d,p) cross sections obtained in this work. At $E_d/2 \sim 12$ MeV these deviations were no more than 4%, while at a larger energy range, $5 \leq E \leq 56$ MeV they could be up to 23%. The unknown non-adiabatic corrections to optical n - A and p - A potentials entering the Schrödinger equation for the $A + n + p$ model [6] can change both real and imaginary parts of these effective potentials, which could affect the (d,p) cross sections. But given that the adiabatic approximation is a good first choice for the (d,p) reactions, most likely, they will not

explain the 70% difference between the NLDOM predictions and experiment.

The contributions from the remnant term in the (d, p) amplitude (all other terms that are not V_{np}) have been studied in an inert core model, where they were found to be small [40]. We estimated the effect of the remnant term for the $^{40}\text{Ca}(d, p)^{41}\text{Ca}$ reaction at $E_d = 11.8$ MeV using FRESKO [41], which employs the inert core approximation and requires the use of local-equivalent potentials. We also found the effect of the remnant term to be small, decreasing the cross section by about 3%. A more recent study [42] showed that the remnant term contributions remain small even when incorporating core-excitation effects, although they can become more important for nuclei in which the core has a low excitation energy. Whether these contributions remain small for a nonlocal U_p is not known.

The strong overestimation of the $^{40}\text{Ca}(d, p)^{41}\text{Ca}$ cross sections at 11.8 MeV implies that neglected parts of the (d, p) amplitude and/or its constituents are much more important than was thought before. Given that the deuteron energy, chosen for this work, is often used in modern experiments with radioactive beams for spectroscopic and astrophysical reasons, and that the dispersive effects are strong at this energy, further development of direct reaction theories is crucial to understand transfer experiments performed either recently or in the past and planned for the future.

ACKNOWLEDGMENT

N.K.T. gratefully acknowledges support from the UK STFC through Grant No. ST/L005743/1. We are grateful to R.C. Johnson for fruitful discussions. S.J.W. would also like to thank W. H. Dickhoff and M. H. Mahzoon for fruitful discussions.

-
- [1] G. R. Satchler, *Direct Nuclear Reactions* (Oxford University Press, New York, 1983), pp. 819–824.
- [2] R. C. Johnson and Tandy, *Nucl. Phys. A* **235**, 56 (1974).
- [3] A. M. Moro, F. M. Nunes, and R. C. Johnson, *Phys. Rev. C* **80**, 064606 (2009).
- [4] A. Deltuva, *Phys. Rev. C* **91**, 024607 (2015).
- [5] A. Deltuva and A. C. Fonseca, *Phys. Rev. C* **79**, 014606 (2009).
- [6] R. C. Johnson and N. K. Timofeyuk, *Phys. Rev. C* **89**, 024605 (2014).
- [7] N. K. Timofeyuk and R. C. Johnson, *Phys. Rev. C* **87**, 064610 (2013).
- [8] M. M. Giannini, G. Ricco, and A. Zucchiatti, *Ann. Phys. (N.Y.)* **124**, 208 (1980).
- [9] M. H. Mahzoon, R. J. Charity, W. H. Dickhoff, H. Dussan, and S. J. Waldecker, *Phys. Rev. Lett.* **112**, 162503 (2014).
- [10] A. Ross, L. J. Titus, F. M. Nunes, M. H. Mahzoon, W. H. Dickhoff, and R. J. Charity, *Phys. Rev. C* **92**, 044607 (2015).
- [11] F. Perey and B. Buck, *Nucl. Phys.* **32**, 353 (1962).
- [12] H. Dussan, S. J. Waldecker, W. H. Dickhoff, H. Mütter, and A. Polls, *Phys. Rev. C* **84**, 044319 (2011).
- [13] W. H. Dickhoff and D. Van Neck, *Many-Body Theory Exposed!*, 2nd ed. (World Scientific, Singapore, 2008).
- [14] H. Fiedeldey, *Nucl. Phys.* **77**, 149 (1966).
- [15] N. Michel, *Eur. Phys. J. A* **42**, 523 (2009).
- [16] J. F. Dicello, G. Igo, W. T. Leland, and F. G. Perey, *Phys. Rev. C* **4**, 1130 (1971).
- [17] R. H. McCamis *et al.*, *Phys. Rev. C* **33**, 1624 (1986).
- [18] L. N. Blumberg, E. E. G. Gross, A. van der Woude, A. Zucker, and R. H. Bassel, *Phys. Rev.* **147**, 812 (1966).
- [19] T. Noro, H. Sakaguchi, M. Nakamura, K. Hatanaka, F. Ohtani, H. Sakamoto, and S. Kobayashi, *Nucl. Phys. A* **366**, 189 (1981).
- [20] D. Y. Pang, F. M. Nunes, and A. M. Mukhamedzhanov, *Phys. Rev. C* **75**, 024601 (2007).
- [21] J. M. Mueller *et al.*, *Phys. Rev. C* **83**, 064605 (2011).
- [22] C. H. Johnson, D. J. Horen, and C. Mahaux, *Phys. Rev. C* **36**, 2252 (1987).
- [23] C. Mahaux and R. Sartor, *Adv. Nucl. Phys.* **20**, 1 (1991).
- [24] M. L. Goldberger and K. M. Watson, *Collision Theory* (Wiley, New York, 1964).
- [25] N. K. Timofeyuk and R. C. Johnson, *Phys. Rev. C* **59**, 1545 (1999).
- [26] D. Y. Pang, N. K. Timofeyuk, R. C. Johnson, and J. A. Tostevin, *Phys. Rev. C* **87**, 064613 (2013).
- [27] L. J. Titus, F. M. Nunes, and G. Potel, *Phys. Rev. C* **93**, 014604 (2016).
- [28] N. K. Timofeyuk and R. C. Johnson, *Phys. Rev. Lett.* **110**, 112501 (2013).
- [29] M. M. Giannini and G. Ricco, *Ann. Phys.* **102**, 458 (1976).
- [30] N. B. Nguyen, F. M. Nunes, and R. C. Johnson, *Phys. Rev. C* **82**, 014611 (2010).
- [31] J. A. Tostevin, University of Surrey version of the code TWOFNR (of M. Toyama, M. Igarashi, and N. Kishida), <http://www.nucleartheory.net/NPG/code.htm>
- [32] N. K. Timofeyuk, *Phys. Rev. C* **84**, 054313 (2011).
- [33] N. K. Timofeyuk, *Phys. Rev. Lett.* **103**, 242501 (2009).
- [34] U. Schmidt-Rohr, R. Stock, and P. Turek, *Nucl. Phys.* **53**, 77 (1964).
- [35] Y. Tian, D.-Y. Pang, and Z.-Y. Ma, *Int. J. Mod. Phys. E* **24**, 1550006 (2015).
- [36] R. L. Varner, *Phys. Rep.* **201**, 57 (1991).
- [37] J. D. Harvey and R. C. Johnson, *Phys. Rev. C* **3**, 636 (1971).
- [38] R. C. Johnson and P. J. R. Soper, *Phys. Rev. C* **1**, 976 (1970).
- [39] F. M. Nunes and A. Deltuva, *Phys. Rev. C* **84**, 034607 (2011).
- [40] W. R. Smith, *Nucl. Phys. A* **130**, 657 (1969).
- [41] I. J. Thompson, *Comput. Phys. Rep.* **7**, 167 (1988).
- [42] M. Gómez-Ramos, A. M. Moro, J. Gómez-Camacho and I. J. Thompson, *Phys. Rev. C* **92**, 014613 (2015).